Aging after shear rejuvenation in a soft glassy colloidal suspension: Evidence for two different regimes

F. Ianni,[1,2,*] R. Di Leonardo,[2] S. Gentilini,[1] and G. Ruocco[1,2]

[1]*Dipartimento di Fisica, Università di Roma "La Sapienza," I-00185 Roma, Italy*
[2]*SOFT-INFM-CNR, c/o Università di Roma "La Sapienza," I-00185 Roma, Italy*

The aging dynamics after shear rejuvenation in a glassy clay suspension have been investigated through dynamic light scattering (DLS). Two different aging regimes are observed: one is attained if the sample is rejuvenated before its gelation and one after the rejuvenation of the gelled sample. In the first regime, the application of shear fully rejuvenates the sample, as the system dynamics soon after shear cessation follow the same aging evolution characteristic of standard aging. In the second regime, aging proceeds very fast after shear rejuvenation, and classical DLS cannot be used. An original protocol to measure an ensemble-averaged intensity-correlation function is proposed and its consistency with classical DLS is verified. The fast aging dynamics of rejuvenated gelled samples exhibit a power-law dependence of the slow relaxation time on the waiting time.

PACS number(s): 83.80.Hj, 83.85.Ei

I. INTRODUCTION

Soft glassy colloidal suspensions are widespread in nature and are of broad technological importance. Macroscopically, they are characterized by a non-Newtonian rheology and, often, by a viscosity that increases many orders of magnitude as time evolves and the gelation process proceeds [1]. These complex fluids also exhibit a strong sensitivity to external forces and have mechanical properties typical of soft solids, such as solidlike behavior below a finite yield stress and thixotropic response to applied deformation [2]. In particular, a shear flow may induce a thinning effect and reduce the fluid viscosity. At the microscopic level, the gelation process corresponds to a slowing down of the structural relaxation with the elapsed time: such a behavior is called aging. Moreover, the system structural dynamics are accelerated by the shear flow. This phenomenon is called shear rejuvenation. The competition between the thickening (produced by the aging) and the thinning (induced by shear flow) gives rise to interesting phenomena.

On the theoretical and numerical side, evidences of the competition between these two effects come from the extension of slow dynamics theories in complex systems, such as mode coupling theory [3], mean-field models [4], trap models [1], and molecular dynamics simulations [5–7], to the presence of external driving forces. These studies show that the structural dynamics are very sensitive to even moderate shear rates, which lead the system to a stationary state. The correlation function in this state is found to decay to zero on a time scale given by $\dot{\gamma}^{-1}$.

On the experimental side, the investigation of the shear-influenced slow dynamics at the microscopic level is still relatively poor. Diffusing wave spectroscopy (DWS) [8–10] and Light-scattering echo (LSE) experiments [11,12] gave indirect evidences for a shear dependent structural relaxation time and for rejuvenation of aged samples. Unfortunately, the statistical properties of multiple-scattered light (probed in DWS and LSE experiments) are not easily represented in terms of the particles' correlation functions. On the contrary, the dynamic light-scattering technique in the single-scattering regime (DLS) probes the intermediate scattering function of the colloidal particles $F_q(t)$ [13], which plays a central role in both theoretical and numerical approaches. In a glassy colloidal suspension, $F_q(t)$ exhibits two decays: a fast relaxation, which accounts for single particle diffusion, and a slow relaxation, whose characteristic time scale τ_s grows many orders of magnitude with the waiting time t_w and accounts for the structural rearrangements of the system. At long t_w, the system enters a glass or gel phase; only the fast relaxation remains and is observed as a decay towards a plateau, reflecting the onset of structural arrest.

On the samples' side, among others, proper candidates for the study of the aging and rejuvenation phenomena in soft glassy colloids are suspensions of charged anisotropic colloidal particles such as clay, which have been widely investigated both for their important industrial application [15,16] and as a prototype of soft glassy materials [17,19,20]. The rejuvenation effect of a shear flow on such systems has been investigated using DWS [8,10], LSE [12], and DLS [22]. The particles' dimension, the sample's history and the kind of shear applied vary among these works; consequently, the effects of shear rejuvenation on the aging dynamics changes and a comprehensive picture of the phenomenology has not yet been reached. In Refs. [22,23], a suspension of Laponite, 25-nm-diam-charged discoidal particles, is used and the waiting time is set to zero after sample filtration. Standard aging in such a sample is characterized by an intermediate scattering function having a stretched exponential slow relaxation, whose characteristic time τ_s grows exponentially with waiting time t_w while becoming strongly stretched. The system dynamics are affected by a steady shear flow, as a strong reduction of aging is evidenced as soon as τ_s enters the time scale set by the inverse shear rate. In Refs. [10,12], aged samples of Saponite particles, 125-nm-diam-charged platelets, are rejuvenated by a strong oscillating shear, after

___
*Electronic address: francesca.ianni@phys.uniroma1.it

which the counting of t_w starts. Under these conditions, aging is much faster and the structural relaxation time exhibits a power-law dependence on t_w.

In this paper, we aim to elucidate the apparently contrasting behavior observed in the two previously described systems [10,12,22,23]. We investigate the aging dynamics following shear rejuvenation in an aqueous suspension of Laponite, before and after the sample gelation occurs. For the regime before gelation, the aging process is investigated through the DLS technique. On the contrary, classical DLS could not be used to follow the dynamics after rejuvenation of gelled samples: aging proceeds very fast in this regime and the system would not be stationary during the acquisition time of a DLS measurement. Therefore, a protocol of DLS acquisition, consisting in an ensemble average over many rejuvenating experiments, is proposed to measure the intensity-correlation function, and its coherence with classical DLS is checked. As a result, we find the existence of two different regimes of aging after shear rejuvenation. If the shear is applied before sample gelation is completed, the rejuvenation is followed by a slow aging regime, behaving just like standard aging after sample preparation. On the contrary, when a gelled sample is rejuvenated by shear, we observe a fast-aging regime after shear cessation, characterized by a power-law dependence of the slow relaxation time on the waiting time.

II. MATERIALS AND METHODS

Many natural clay mineral particles, such as hectorite and bentonite, or synthetic clay particles such as Laponite, have a disk-shaped crystal structure, with a characteristic chemical structural formula and size. When dispersed in a polar solvent, these anisotropic particles release counterions and get differently charged on the edge and on the faces of the crystal disk. The strong electric field generated by the bare charge of the colloidal particles attracts the free charges, which remain tightly bounded to the surface of the colloids, forming a layer of condensed counterions. The resulting screened charged interactions between the particles are not trivial. Aqueous suspensions of Laponite, a synthetic layered silicate, composed of monodisperse discoidal particles (with a diameter of 25 nm and a 1 nm thickness), have been extensively investigated as a model system for disklike charged colloids. Diverse theoretical and numerical works [18] have been devoted to the study of this complex system and the formation of a disordered arrested phase even at very low volume fractions has been evidenced, as confirmed by experiments [17,19,20]. Moreover, for sufficiently concentrated samples, a two-stage aging process has been observed experimentally through the DLS technique [21]: for small t_w, the structural relaxation time τ increases exponentially (or more than exponentially), with t_w, while for long t_w, when $\tau > t_w$, a power-law behavior shows up.

For our experiments, Laponite powder provided by Laporte Ltd is dispersed in ultrapure water at 3% wt concentration and stirred for ~ 30 min. The obtained suspension, which is optically transparent and initially "liquid," is loaded into a homemade, cone and plate shear cell for DLS mea-

surements, having a flat optical window as the static plate. Cell loading (through a 0.45 μm filter) is taken as the origin of waiting times for standard aging. Incident laser beam (diode pumped solid-state laser, $\lambda = 532$ nm, $P = 150$ mW) and scattered light pass through the same optical window. The scattered light is collected by a monomode optical fiber and detected by a photomultiplier, after being optionally mixed with a coherent local oscillator field. Photocounts are acquired through a general purpose, counter (timer) PCI board (National Instruments PCI 6602). We developed a set of software classes (implemented as extension modules of the object-oriented language Python) designed to perform basic tasks for the statistical analysis of digital pulse trains. A typical application is real time multi-tau photon correlation. However, a software approach, having access to the full photocounts train, allows one to efficiently prototype different analysis protocols, going far beyond the simple autocorrelation function [24]. The scattering geometry is fixed (scattering vector $q = 22$ μm^{-1}). The shift of the cell allows us to select the position of the scattering volume in the cell gap and the possibility of choosing a heterodyne correlation scheme [25] enables direct access to the detailed velocity profile in the shear cell.

The aging dynamics of the system is investigated through the DLS technique, which allows direct access to the intermediate scattering function. More specifically, the normalized intensity autocorrelation function $g^{(2)}(t_w,t) = \langle I(q,t_w)I(q,t_w+t)\rangle_T / \langle I(q,t_w)\rangle_T^2$ is measured as an average on the time origin, $\langle\ldots\rangle_T$ indicating temporal average over the acquisition time T. In the single-scattering regime and within the Gaussian approximation $g^{(2)}(t_w,t) = 1 + |F_q(t_w,t)|^2$ [13], where $F_q(t_w,t) = \langle \rho_{-q}(t_w)\rho_q(t_w+t)\rangle / \langle \rho_{-q}(t_w)\rho_q(t_w)\rangle$ is the intermediate scattering function of the colloidal particles. The experimental acquisition time T needed to get a good signal-to-noise ratio must be kept longer than the characteristic slow relaxation time of the system τ_s and shorter than the time one should wait before changes in τ_s, due to the aging process, are significant. This condition does not hold when the aging dynamics is characterized by a very fast evolution, as in one of the two regimes of aging that we want to investigate. The intensity-correlation function thus cannot be obtained by time averaging and an ensemble average may overcome the problem. Multispeckle dynamic light scattering (MS-DLS) or multispeckle diffusive wave spectroscopy (MS-DWS) compute the intensity-correlation function by averaging the intensity fluctuations over the pixels of a digital camera detector, which collects part of the speckle pattern [14]. The acquisition time is strongly reduced in these techniques, enabling the investigation of the system dynamics for much longer τ_s or for faster aging processes. However, in both techniques, the time resolution is much smaller than in DLS, as it is limited by the frame rate of the camera device used as detector. In particular, the time scale characterizing the slow dynamics of the Laponite suspension in the regime we are interested in may be too short to be investigated through MS-DLS.

In our experiment, an ensemble average over many rejuvenating experiments is used: $g^{(2)}(t_w,t) = \langle I(q,t_w)I(q,t_w+t)\rangle_e / \langle I(q,t_w)\rangle_e^2$, where $\langle\ldots\rangle_e$ indicates the ensemble average

over several intensity evolutions acquired after cessation of a repeated shear application. In particular, we choose the following protocol: a shear rate $\dot{\gamma}_1$ is applied to the system for a time interval T_1; after shear cessation, the intensity fluctuations are collected for a time interval T_0 with a time resolution of dt; then a shear rate of the same value $\dot{\gamma}_1$ is applied for T_1 and the cycle starts again. The whole measurement lasts several hours and we obtain an ensemble of N acquisitions, having T_0/dt counts each, after the same initial conditions are imposed. In order to reach a good signal-to-noise ratio in the correlation function, N needs to be large. For this reason, the acquisition time is extremely long in comparison to the MS-DLS technique, but the time resolution, fixed by dt, can be much higher with this DLS technique and enables the investigation of faster dynamics. Once the counts have been collected, we proceed to the calculation of the correlation functions. To speed up the computation, the acquired counts are first logarithmically binned: a logarithmic binning of t_w is performed and the counts are averaged in each bin. The intensity autocorrelation function is then calculated as an ensemble average over all the bunches of counts, in the time window $dt-T_0$: calling $n_i(t_w+t)$ the number of counts in the bin at the elapsed time t_w+t since shear cessation and at the ith acquisition, we can write

$$g^{(2)}(t_w,t) = \frac{1}{N} \frac{\sum_{i=1}^{N} n_i(t_w)n_i(t_w+t)}{\bar{n}^2},$$

where $\bar{n}$ is the average of all the counts in all the N acquisitions.

In order to follow the statistics of the correlation functions for various t_w [14], we calculated for each acquisition i the value $n_i(t_w)n_i(t_w+\bar{t})/\bar{n}^2$ at different t_w, with $\bar{t}$ satisfying the condition $g^{(2)}(t_w,\bar{t})=e^{-1}$. A histogram of these values calculated for the N acquisitions can be plotted for each t_w [Fig. 1 (inset)]. Its shape, though very large, ensures that good statistics have been done in the calculation of the correlation function.

Finally, consistency with classical DLS has been checked for this original method of DLS, employed to measure the intensity-correlation function for a rapidly aging sample. In order to compare the correlation functions measured through both methods, we monitored the aging dynamics of a Laponite sample under shear at short elapsed time t_w^0 since sample filtration. In this regime, the system dynamics after shear rejuvenation are stationary over the time scale of the tens of seconds and can thus be investigated through classical DLS also. Soon after cell loading, the sample is left aging under shear at $\dot{\gamma}_1=100$ s^{-1} and periodically shear is stopped after a time $T_1=60$ s, a pause of 5 s is taken in order to avoid inertial effects due to flow stop, and then the scattered intensity is acquired for $T_0=1$ s, with a time resolution $dt=10^{-5}$ s. Each hour, the time-averaged intensity-correlation function is also measured through classical DLS by stopping the shear for 80 s. The experiment lasts 24 h and the ensemble-averaged intensity-correlation function is calculated from the $N=1300$ acquired bunches of counts. As the system under
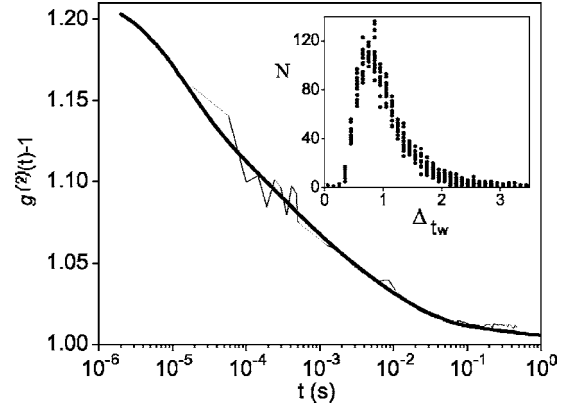

FIG. 1. Intensity-correlation function measured as an ensemble average over many intensity acquisitions after shear cessation (thin line) compared to the time-averaged correlation function measured through classical DLS (bold line). Measurements are performed on a Laponite sample aging under shear at $\dot{\gamma}_1=100$ s^{-1} for 24 h. As the sample ages during this long acquisition time, the correlation function plotted in a bold line is an average of all the correlation functions acquired during the experiment through classical DLS. *Inset*: For 14 waiting times values between 1 and 80 s, we plot the histograms of $\Delta_{t_w}=n_i(t_w)n_i(t_w+\bar{t})/\bar{n}^2$ (with $\bar{t}$ satisfying the condition $g^{(2)}(t_w,\bar{t})=e^{-1}$) calculated for each acquisition i among $N=950$ acquisitions.

shear keeps on aging with t_w^0 [22], the dynamics change during the whole experiment and the ensemble-averaged correlation function will provide an average value of the slow relaxation time scale. The ensemble-averaged intensity-correlation function is thus compared to the average of all the intensity-correlation functions measured during the experiment through classical DLS (Fig. 1). In conclusion, good agreement is observed between the intensity-correlation functions measured through the two methods.

III. RESULTS

A. Standard aging and gelation

We first follow the standard aging evolution of the sample after cell loading, calling t_w^0 the time elapsed since sample filtration. The dynamics is monitored by measuring the intensity-correlation function in the time window $10^{-6}-1$ s through classical DLS [23]. A two-step decay for $F_q(t_w,t)$ is observed during the aging and a very good fit for all the correlations is provided by

$$F_q(t_w,t) = f \exp[-(t/\tau_s)^\beta] + (1-f)\exp[-t/\tau_f], \quad (1)$$

where all parameters (f,τ_s,β,τ_f) depend on t_w^0. As the waiting time t_w^0 evolves, the slow relaxation decay becomes more stretched: the stretching parameter β is smaller than one and decreases with t_w. In order to quantify the slow decay time scale, we calculate the average slow relaxation time $\langle\tau_s\rangle$ ($\langle\tau_s\rangle=\int_0^\infty \exp[-(t/\tau_s)^\beta]dt=\tau_s/\beta\Gamma(1/\beta)$, where Γ is the Euler gamma function) and we plot it as a function of t_w^0 in Fig. 2 (open circles). The evolution of the fast relaxation time scale τ_f exhibits a slow increase with t_w^0, as plotted in the inset of Fig. 2.
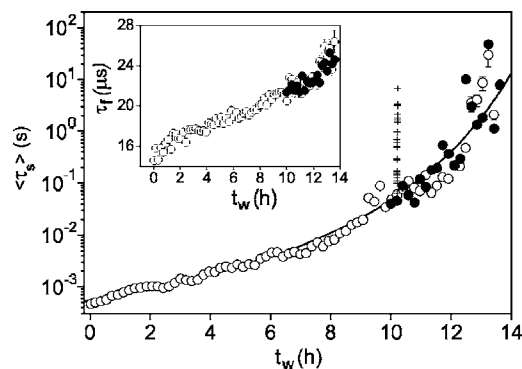
FIG. 2. Average slow relaxation time $\langle \tau_s \rangle$ is plotted as a function of waiting time t_w for a sample aging soon after filtration ($\bigcirc$) and for the same sample aging after the application of a shear rate of 100 s^{-1} for 2 min, 13.4 h after filtration ($\bullet$). t_w is shifted in order to superimpose the first $\langle \tau_s \rangle$ measured after the application of shear with the standard aging curve. The black line is a guide for the eye. The fast aging regime, observed after shear rejuvenation of a gelled sample, is also plotted for comparison for the same applied shear rate (+). The curve is shifted in t_w through the above-described procedure. *Inset*: fast relaxation time τ_f as a function of t_w for the two aging evolutions, plotted through the same procedure.

At a given t_w^0, the slow relaxation of the correlation function does not show a complete decay within the time window explored and the slow relaxation time cannot be defined any more. This behavior indicates a strong ergodicity breaking and marks conventionally the crossover to the arrested phase [19]. With the time window accessible in our DLS experiment, gelation takes place in our sample at $t_w^0 \sim 18$ h. A very rapid increase of the slow relaxation time is indeed evident just before gelation in Fig. 2.

B. Rejuvenation before gelation

We now investigate the aging dynamics that follows the shear rejuvenation induced before full gelation of the sample. We let the system age until $t_w^0 = 13.4$ h, then we apply a shear rate of 100 s^{-1} for two minutes and finally, we follow the dynamics after shear cessation through DLS. We define t_w as the time elapsed since shear cessation. Aging is monitored through the intensity autocorrelation function $g^{(2)}(t_w, t)$ for a set of t_w between 0.2 and 3 h, as reported in Fig. 3 (left panel). The correlation functions have the same shape observed in the standard aging regime and can still be fitted through the expression of Eq. (1). The stretching parameter β decreases with t_w, as shown in the left panel of Fig. 4. The evolution of $\langle \tau_s \rangle$ as a function of t_w is plotted in Fig. 2 (full circles), where the t_w axis has been shifted by superimposing the first point of the curve on the standard aging curve. As evidenced in the figure, once a shorter relaxation time is reached by the system through the rejuvenating effect of the shear, the same aging evolution characteristic of standard aging is followed. The same behavior can be observed in the evolution of the fast relaxation time scale τ_f, which is plotted in the inset of Fig. 2.

C. Rejuvenation after gelation

We now turn to the investigation of the aging evolution after the shear is applied to gelled samples. When a local
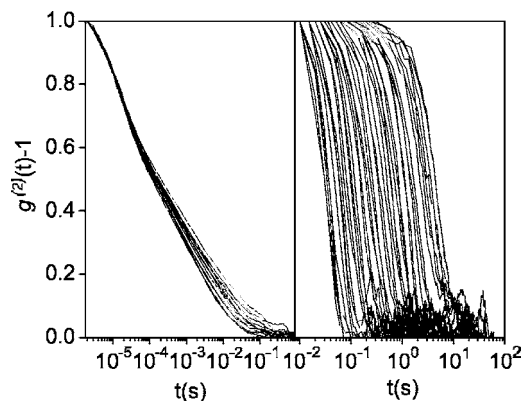

FIG. 3. Normalized intensity-autocorrelation functions for two different aging regimes after shear rejuvenation. *Left*: a Laponite sample rejuvenated before entering the arrested phase. Correlation functions are obtained through an average on the time origin for 16 equally spaced waiting times t_w^0 between 0.2 and 3 hours (from left to right) after shear cessation. *Right*: a gelled Laponite sample for a set of t_w^0 between 0.3 and 40 s (from left to right) after shear cessation. Correlation functions are obtained through the ensemble-average procedure. In this last case, the fast decay is not accessible.

shear rate $\dot{\gamma}_1$ is applied to the system, the scattered intensity following shear cessation shows the type of evolution reported in Fig. 5, where t_w is the time elapsed since flow stop. The fluctuations of the signal display a rapid slowing down within the plot time window. In particular, the fluctuations look stationary in a log-linear plot of the intensity evolution, as shown in the bottom panel of the figure. For such a rapid evolution of the dynamics, the intermediate scattering function will be monitored by measuring an ensemble-averaged correlation function through the method described in Sec. II.

We first want to point out that aged samples always exhibit wall slip on the static plate (optical window). In particular, when a still, gelled Laponite suspension is put under shear, drastic wall slip takes place and the whole system rotates as a solid body leaving a null shear in the core (measurements of the velocity profile are performed through the
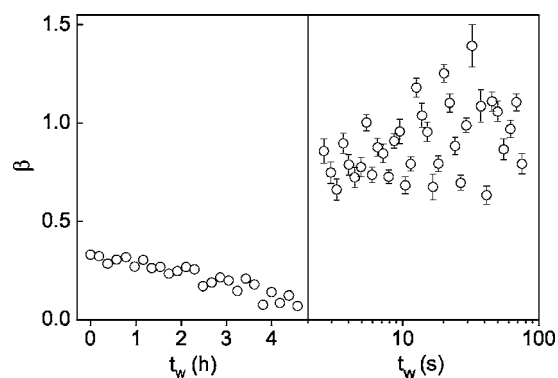

FIG. 4. Difference of the two aging regimes after shear rejuvenation as evidenced from the evolution of the β parameter, deduced from a stretched exponential fit $\exp[(-t/\tau_s)^\beta]$ of the intensity-autocorrelation function. *Left*: aging of a sample rejuvenated before entering the arrested phase. *Right*: aging of a rejuvenated gelled sample.
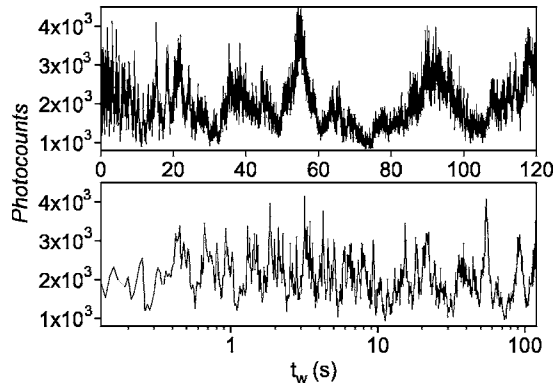
FIG. 5. Fast slowing down of the scattered intensity fluctuations with the waiting time for a rejuvenated gelled Laponite sample. *Top*: the evolution of the counts revealed by the photomultiplier in 10^{-2} s soon after shear cessation is plotted, $t_w=0$ corresponds to the shear stop. *Bottom*: log-linear plot of the counts evolution; a logarithmic binning of t_w has been performed and the counts have been averaged in each bin.

FIG. 6. Aging after rejuvenation of a gelled Laponite sample. The evolution with t_w of the slow relaxation time τ_s is plotted for various applied shear rates $\dot{\gamma}_1$: ($\diamond$) 6 s^{-1}, ($\square$) 28 s^{-1}, ($\blacktriangle$) 66 s^{-1}, ($\circ$) 134 s^{-1}. The curves do not show significant variations for the different $\dot{\gamma}_1$. The bold line is a fit to a $t_w^{-1.2}$ power law.

heterodyne dynamic light-scattering setup [25]). In order to apply a controlled shear rate, the solid band is broken through the application of a high shear rate ($\dot{\gamma}_0 > 100$ s^{-1}). A local shear rate $\dot{\gamma}_1 < \dot{\gamma}_0$ can be applied soon after to investigate aging after shear through the ensemble-average procedure. Another protocol consists in letting the system age under continuous shearing. Though wall slip is still present at the lower shear rates investigated ($\dot{\gamma}_1 \ll \dot{\gamma}_0$), velocity profiles show a finite local shear rate. We found that, for a given local shear rate, the subsequent aging dynamics is independent on which of the two described protocols is applied. In the following, we will always refer to samples prepared according to the first procedure.

Various experiments at different $\dot{\gamma}_1$ will be performed, with the following parameters for the measuring protocol: $\dot{\gamma}_0 = 200$ s^{-1} and its application lasts two minutes, $T_1 = T_0 = 120$ s and $dt = 10^{-2}$ s. The time resolution, which is fixed by dt, has been chosen in order to let us follow the slow dynamics, while limiting the time spent in the computation of the correlation functions (the number of counts for each acquisition is T_0/dt). In order to minimize inertial effects due to flow stop, the shear rate $\dot{\gamma}_1$ is set to zero through a decreasing ramp of the duration of 10 s. The resulting $g^{(2)}(t_w, t)$ for a set of waiting times between 1 and 40 s are reported in Fig. 3 (right frame). In order to show that aging of the sample under shear [22] is negligible during the whole experiment, we also calculate the correlation functions by taking only the first or last group of acquired counts and obtain the same results. The ensemble-averaged correlation functions are first fitted by a stretched exponential decay, the fast component of dynamics being below the present time window. Results of the data analysis are checked to be invariant under different binning and fitting procedures.

Compared to standard aging, the new aging regime entered by the rejuvenated gelled sample is characterized by correlation functions of a different form and by a much more rapid evolution of the slow relaxation time with t_w. In particular, from a stretched exponential fit, the stretching param-
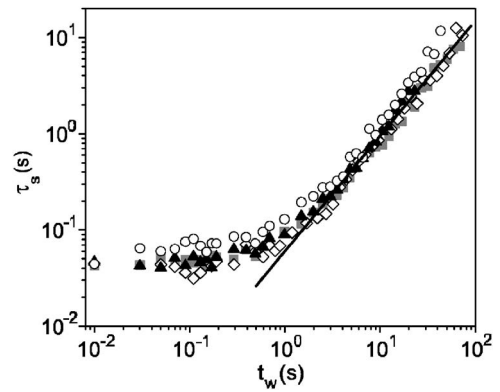
eter of the correlation function statistically fluctuates around one and does not seem to depend on the waiting time (Fig. 4, right panel). For a given t_w, the slow relaxation time is then obtained as the value τ_s satisfying the condition: $g^{(1)}(\tau_s, t_w) = 0.5$. Results are checked to be consistent with other fitting procedures. The obtained curves of τ_s vs t_w for various $\dot{\gamma}_1$ in the range 6–134 s^{-1} are reported in Fig. 6. A plateau is evident at short t_w, while a power-law behavior is found at longer t_w: $\tau_s \sim t_w^c$. No significant difference is observed in the aging evolution as the applied shear rate varies in the range here investigated. In particular, the slow relaxation time soon after flow stop can be quantified by the plateau value, which does not show any dependence on $\dot{\gamma}_1$. The two regimes of aging investigated are compared by adding, in Fig. 2, the plot of the slow relaxation-time evolution in this second regime (crosses): aging is so fast that the curve seems to diverge instantaneously with the time resolution fixed by the first regime.

IV. DISCUSSIONS AND CONCLUSIONS

Regarding the standard aging regime, we want to highlight the dependence of the fast relaxation time on the waiting time, which is also confirmed in the aging evolution after shear rejuvenation in the first regime investigated, i.e., before sample gelation. This result indicates a common origin of the fast and slow relaxation in Laponite suspensions, but is in disagreement with previous observations [20,21], that showed the independence of the fast dynamics on the age of the sample and the scaling of the fast relaxation time with q^{-2}. In these previous works, the first decay of the correlation function is interpreted as an evidence of single-particle diffusion, while the slow decay accounts for collective dynamics. Further investigations are needed to clarify this point.

We now turn to the discussion on the rejuvenating effect of the shear flow and on the following aging dynamics. Once a shear is applied before gelation of the sample, a reduced relaxation time scale is observed soon after shear stop. This starting value depends on the applied shear rate: fixing the

time t_w^0 when the shear is applied, we expect that τ_s soon after shear cessation scales as the inverse shear rate [22]. The following evolution of the relaxation times (both fast and slow) traces the same aging curves (once the waiting time axis is shifted) exhibited during standard aging, showing that aging is reversible in this regime and true rejuvenation is achieved through shear flow.

After shear rejuvenation of a sample in the arrested phase, the system dynamics is no longer reversible: the aging process that has induced the arrested phase cannot be reached again through shear rejuvenation, and a completely different regime is reached. The intensity-correlation function characterizing the dynamics in this new regime exhibits a simple exponential decay, differently to what happens in the other regime. The approximate scaling of the slow relaxation time as the inverse shear rate, suggested by the schemes usually applied to glassy systems [1,3–7], is no longer valid. On the contrary, in the range of shear rates here investigated (spanning more than one decade), the slow relaxation time after flow stop does not seem to depend on the applied shear rate. Therefore, at the lower shear rates, the flow exhibits a surprisingly strong rejuvenating effect, with the slow relaxation time-scale getting shorter than the inverse shear rate after flow stop. Then, the system quickly ages back to the arrested state. After a plateau region (evident in a logarithmic plot), a power-law dependence of the slow relaxation time with waiting time is observed for long t_w, with exponent $c \sim 1.2$. Such a behavior (with two different regimes for short and long t_w) has already been observed after rejuvenation of other colloidal glasses [9]. In other clay suspensions similar to Laponite, a power-law behavior of τ_s vs t_w, with an exponent close to one, has been observed after shear rejuvenation of aged samples [10,12]. However, we could not find for these systems any information in the literature about standard aging, or aging after rejuvenation of young samples. It would be interesting to find out whether a different, slower aging process is observed in these regimes, as it happens in Laponite suspensions, and if the described phenomenology can be generalized to charged discoidal colloids. Finally, the same power-law behavior has also been observed during the standard aging of Laponite suspensions at very long waiting times [21].

The phenomenology observed in the second regime of aging after shear rejuvenation is not well understood. If the arrested phase at the concentration here investigated corresponds to a glassy phase, the observed behavior of the slow relaxation time as a function of the shear rate would be totally unexpected. Actually, a debate on the arrested phase of Laponite suspensions is still open [26–29] and it is not clear yet whether a gel phase or glassy phase occurs in the system. The unexpected scaling of $\tau_s(t_w \to 0)$ with $\dot{\gamma}$ and the following rapid aging evolution may thus be interpreted through the formation of a gel, characterized by the existence of a fractal network [27]. In this context, Ref. [30] suggests that the decorrelation of the scattered light would not be due to the dynamics of single scatterers, but to a drift mechanism of big aggregates of particles.

In conclusion, we have shown the existence of two different regimes of aging for a suspension of charged discoidal clay particles after shear rejuvenation. Before gelation, classical DLS measurements have shown that a shear flow can fully rejuvenate the sample. The system dynamics soon after shear cessation depend on the applied shear rate, with the slow relaxation time scaling as the inverse shear rate [22], while the following aging evolution is identical to the one after sample preparation: the fast relaxation time increases slightly with the waiting time t_w, while the slow relaxation time grows exponentially with t_w and becomes strongly stretched. On the contrary, in a gelled sample, aging dynamics after shear rejuvenation proceeds very rapidly, so classical DLS measurements cannot be used and a dynamic light-scattering method to measure the intensity-correlation function has been proposed. An ensemble average over many rejuvenating experiments is used and the validity of this method is checked through comparison with classical DLS measurements. With this method, we observed an intensity correlation function characterized by a single exponential decay, differently from the other regime. Moreover, the scaling of the slow relaxation time scale soon after shear cessation as the inverse shear rate is no longer valid in this regime. After a plateau region, the slow relaxation time scale shows a power-law dependence on t_w. Further studies are needed to clarify the nature of this aging evolution after shear rejuvenation and how it is linked to the gelation process.

[1] P. Sollich, F. Lequeux, P. Hébraud, and M. E. Cates, Phys. Rev. Lett. **78**, 2020 (1997).

[2] R. G. Larson, *The Structure and Rheology of Complex Fluids* (Oxford University Press, New York, 1999).

[3] M. Fuchs and M. E. Cates, Phys. Rev. Lett. **89**, 248304 (2002).

[4] L. Berthier, J.-L. Barrat, and J. Kurchan, Phys. Rev. E **61**, 5464 (2000).

[5] R. Yamamoto and A. Onuki, J. Chem. Phys. **117**, 2359 (2002).

[6] L. Berthier and J.-L. Barrat, J. Chem. Phys. **116**, 6228 (2002).

[7] L. Angelani, G. Ruocco, F. Sciortino, P. Tartaglia, and F. Zamponi, Phys. Rev. E **66**, 061505 (2002).

[8] D. Bonn, S. Tanase, B. Abou, H. Tanaka, and J. Meunier, Phys. Rev. Lett. **89**, 015701 (2002).

[9] V. Viasnoff and F. Lequeux, Phys. Rev. Lett. **89**, 065701 (2002).

[10] F. Ozon, T. Narita, A. Knaebel, G. Debrégeas, P. Hébraud, and J.-P. Munch, Phys. Rev. E **68**, 032401 (2003).

[11] G. Petekidis, A. Moussaïd, and P. N. Pusey, Phys. Rev. E **66**, 051402 (2002).

[12] S. Kaloun, M. Skouri, A. Knaebel, J.-P. Münch, and P. Hébraud, Phys. Rev. E **72**, 011401 (2005).

[13] B. Berne and R. Pecora, *Dynamic Light Scattering* (Wiley, New York, 1976).

[14] L. Cipelletti, H. Bissig, V. Trappe, P. Ballesta, and S. Mazoyer, J. Phys.: Condens. Matter **15**, S257 (2003).

[15] W. Götze and L. Sjögren, Phys. Rev. A **43**, 5442 (1991).

[16] H. Van Olphen, *An Introduction to Clay Colloid Chemistry*, 2nd ed. (Wiley, New York, 1977).

[17] M. Kroon, G. H. Wegdam, and R. Sprik, Phys. Rev. E **54**, 6541 (1996).

[18] L. Harnau, D. Costa, and J.-P. Hansen, Europhys. Lett. **53**, 729 (2001); M. Dijkstra, J.-P. Hansen, and P. A. Madden, Phys. Rev. Lett. **75**, 2236 (1995); R. J. F. Leote de Carvalho, E. Trizac, and J.-P. Hansen, Europhys. Lett. **43**, 369 (1998).

[19] B. Ruzicka, L. Zulian, and G. Ruocco, Phys. Rev. Lett. **93**, 258301 (2004); Langmuir **22**, 1106 (2006).

[20] B. Abou, D. Bonn, and J. Meunier, Phys. Rev. E **64**, 021510 (2001).

[21] M. Bellour, A. Knaebel, J. L. Harden, F. Lequeux, and J.-P. Münch, Phys. Rev. E **67**, 031405 (2003).

[22] R. Di Leonardo, F. Ianni, and G. Ruocco, Phys. Rev. E **71**, 011505 (2005).

[23] R. Di Leonardo, S. Gentilini, F. Ianni, and G. Ruocco, J. Non-Crystalline Solids (to be published).

[24] The PhotonLab package is available for download at: http://glass. phys. uniroma1. it/dileonardo/photonlab. html

[25] R. Di Leonardo, F. Ianni, and G. Ruocco, J. Fluid Mech. **525**, 27 (2005).

[26] D. Bonn, P. Coussot, H. T. Huynh, F. Bertrand, and G. Debrégeas, Europhys. Lett. **59**, 786 (2002).

[27] A. Mourchid and P. Levitz, Phys. Rev. E **57**, R4887 (1998).

[28] T. Nicolai and S. Cocard, Langmuir **16**, 8189 (2000).

[29] D. Bonn, H. Kellay, H. Tanaka, G. Wegdam, and J. Meunier, Langmuir **15**, 7534 (1999).

[30] L. Cipelletti, S. Manley, R. C. Ball, and D. A. Weitz, Phys. Rev. Lett. **84**, 2275 (2000).